Available online at www.sciencedirect.com

ScienceDirect

Journal of the Franklin Institute 359 (2022) 1382–1406

www.elsevier.com/locate/jfranklin

Controlling the variable length pendulum: Analysis and Lyapunov based design methods

Milan Anderle[a], Pieter Appeltans[b], Sergej Čelikovský[a,*], Wim Michiels[b], Tomáš Vyhlídal[c]

[a] *The Czech Academy of Sciences, Institute of Information Theory and Automation (ÚTIA AV ČR), 182 08, Prague 8, Czechia*

[b] *Department of Computer Science, KU Leuven, Celestijnenlaan 200A, Heverlee 3001, Belgium*

[c] *Department of Instrumentation and Control Engineering, and Center of Advanced Aerospace Technology, Faculty of Mechanical Engineering, Czech Technical University in Prague, Technická 4, Prague 6, 166 07, Czechia*

Received 26 July 2021; received in revised form 8 November 2021; accepted 27 November 2021
Available online 8 December 2021

Abstract

The analysis and design of methods to damp the swing of the variable length pendulum by adjusting its length are presented here. To analyze the theoretical limits of such Coriolis force based damping, a comprehensive open-loop numerical analysis is performed for a two-dimensional model having the string length as the controlled input. Further, for a four dimensional model, having the force applied to the string as the controlled input, a smooth static state feedback controller is designed using backstepping. Results are verified both in simulations and through extensive laboratory experiments, and compared with previously published results achievable using an identical experimental setting.

1. Introduction

This paper considers the damping of the swing of a pendulum by adjusting the suspension length. Even though the pendulum-like problem under consideration may seem purely theo-

* Corresponding author.
E-mail addresses: anderle@utia.cas.cz (M. Anderle), pieter.appeltans@kuleuven.be (P. Appeltans), celikovs@utia.cas.cz (S. Čelikovský), wim.michiels@kuleuven.be (W. Michiels), tomas.vyhlidal@fs.cvut.cz (T. Vyhlídal).

https://doi.org/10.1016/j.jfranklin.2021.11.026
0016-0032/

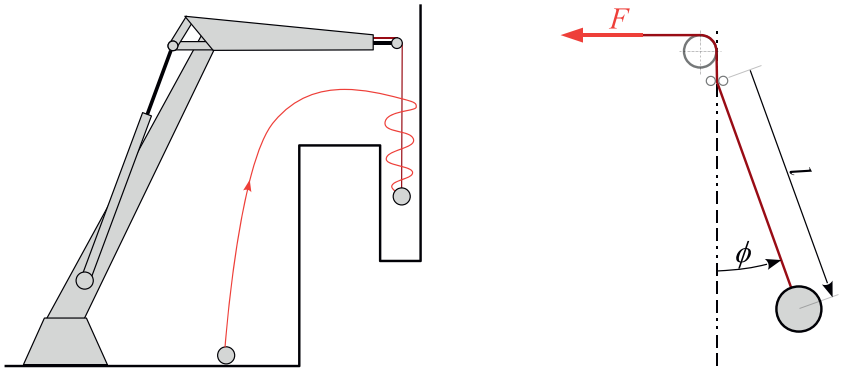

Fig. 1. Left: Problem motivation - damping the residual payload sway at the final stage of a robotic crane maneuver using the Coriolis force acting on the payload; Right: reformulating the problem as controlling the variable length pendulum.

retical, it has a high potential, particularly in crane like applications [1]. The common task of crane control systems is to maneuver a suspended payload from one position to another, while taking into account trajectory constraints, as shown in Fig. 1. An established technique in crane motion control is *input shaping* [2,3], see also [4] for optimal and [5] for robust design. The main idea of this method is to shape the trajectory of the cable suspension point by a time delay filter so that the payload sway is partly or fully pre-compensated. Alternatively, the trajectory of the suspension point can be optimized directly [6,7]. Let us also point to the combined input shaping and feedback control method presented in [8,9], and to the direct feedback control methods proposed in [10] with real-time visual tracking, in [11] by nonlinear tracking control and in [12,13] by an MPC based algorithm. In [14], an online trajectory planning of the jib and the trolley of a double-pendulum tower crane was proposed using Lyapunov's method, LaSalle's invariance Theorem and Babarlat's Lemma.

The presented research is motivated by the need to damp the residual oscillations of a suspended payload at the final stage of a maneuver where the suspension point reaches the end-point position and remains fixed. Such residual oscillations are very likely to appear even when one of the previously mentioned methods is applied, mainly due to control system imperfections or external disturbances. Damping these residual oscillations by further maneuvering the suspension point may be inefficient or even impossible due to physical constraints, as indicated in Fig. 1. In this case, the Coriolis force acting at the payload can be utilized to damp the oscillation by adapting the suspension length during the swing. As also indicated in Fig. 1 the crane problem at hand is equivalent with controlling the variable length pendulum.

Energy based open-loop control design of pendulum swing damping by varying the suspension length can be traced back to [15]. More specifically, [15] and, later on, [16] proposed a harmonic signal for the cable length that is synchronized with the swing motion using additional, non-trivial signal processing tools. Even though this open-loop approach was verified in laboratory experiments, see [17] and [18], it is hardly applicable in practice where the periodic motion may be affected by disturbances. In contrast, the closed-loop control law presented in [19] does not require any additional signal processing as synchronization is guaranteed by feedback of the pendulum angle. Further, a robust optimization procedure and extended linearizations are employed to attenuate oscillations in crane systems by adjusting the cable

length in [20], while in [21] two energy-based methods are proposed to suppress the pendulum's oscillation by simultaneously controlling the pivot point and the position of the weight of the pendulum. A stabilizing control law that damps the swing of a pendulum by controlling the rod length has been developed using a Lyapunov method in [22] and it has been verified in laboratory experiments in [23]. Yet, the variation of the gravity center position was attenuated there in some indirect way only. A Lyapunov based nonlinear control design was also used in [24], which considered a three-dimensional state space model and included a cable length penalty term into the Lyapunov function candidate. For the same three-dimensional model, a control strategy was developed in [25], relying on the concept of passivity, which allows to generate a broad set of Lyapunov function candidates providing various mutually complementary damping performances. In [26], the efficiency of amplitude suppression of an oscillating pendulum by a controllable moving mass was studied by simulations for several suppression rules. Besides, attention was paid to solving the nonsynchronous motion problem identified in [16]. The main recommendation stems in minimization of the pendulum length transition times precisely synchronous with the pendulum position. The problem was further studied and its results were experimentally validated in [27]. In the aforementioned work, instead of varying the cable length, the mass equipped with bearings and driven by a stepping motor via a synchronous belt slides on two rods. Thus, the acceleration of the downward motion is not limited by the gravitational acceleration as it is in the case of controlling directly the cable length.

Let us also point to an analogous problem, recently examined in [28], where the pendulum length is kept fixed and its angular motion is damped by up and down motion of the pivot. In this case, damping is achieved through the momentum effect of the difference between the gravitational and inertia forces on the pendulum bob. In another recent study [29], rapid oscillation suppression is achieved by using phase delay motion of the horizontally movable pivot. The pivot's continuous motion control with a lagging phase difference is realized by taking the pendulum's time delay angle as an input. In [30], considering the varying rope length, the dynamic model of the double pendulum crane system with distributed mass beams is established and controlled in sliding mode sense.

The literature studying variable length pendulums is not limited to damping. As samples of other investigated aspects, let us mention the analysis of the periodic solutions induced by periodically varying the cable length [31,32] and the analysis of the regimes of regular and chaotic motion of the pendulum with the periodically varying cable length [33]. Note also that a similar situation with practically useless friction appears in magnetic manipulation [34]. Though being quite a different application, the respective mathematical model presents some similar features as used in the current paper later on, when analysing the two-dimensional state-space model in a switched systems setting.

The current paper brings two novel contributions to the pendulum swing damping by adjusting its length. The *first contribution* lies in a thorough analysis of the classical set-up considered in literature when the pendulum length, or its derivative, is considered as the control input. Inspired by the numerical solution of an optimal control problem, intended to explore the theoretical limits of damping, a switched feedback control law for adjusting the cable length is proposed and analyzed. Subsequently, this control law is approximated by a smooth feedback law. The asymptotic stability of the resulting close loop is then demonstrated using Lyapunov's method. The *second contribution*, motivated from engineering practise, consists of extending the problem's complexity by considering the force acting on the cable as the control system input. It should be stressed that solving this extended problem considerably simplifies

the implementation of the control law, as in this case, no slave control loop is needed to adjust the cable length, *i.e.,* to exert the force needed to adjust the length. Again, a Lyapunov method is used to prove the asymptotic stability. Further contributions brought by this paper are: i) a thorough study of the state space representations of the two considered settings, and ii) a comparison of the newly proposed methods with selected existing approaches using both simulations and experiments.

The remainder of the paper is organized as follows. Section 2 introduces the problem, presents various possible state-space models and repeats in detail two existing approaches that will be compared to the novel approaches introduced in the paper. The main theoretical and numerical results are presented in Sections 3 and 4. The former presents a thorough study of the theoretical limits of swing damping by adjusting the pendulum length and provides a practical smoothed feedback approximation of the optimal solution. The latter presents the novel control law using the force as the input. This new, realistic feedback control law is thoroughly compared with the previously known approaches using both simulations and experiments in Section 5. The final section briefly concludes the paper and indicates some ongoing and future research directions.

2. Preliminaries and problem formulation

2.1. The problem set-up and its mathematical models

The right-hand side of Fig. 1 depicts schematically the considered set-up. The pendulum length is adjusted by a control force $F(t)$ generated by a servomechanism and acting on the suspension cable. This does not constitute a significant theoretical difference compared to cable rewinding using torque. To model this set-up, the cable's mass and the friction corresponding to the lateral pendulum's swing are neglected. Indeed, the effect of the latter is negligible and would improve damping, not worsen it. On the contrary, the friction related to the contact of the cable at the pivot may have a notable influence on the controller's performance. Its coefficient is assumed to be known and is denoted by κ. Since the cable is moving most of the time, the effect of dry friction at the pivot may be neglected. Clearly, when concentrating on capturing the effect of rather weak quadratic Coriolis forces such a simplification is acceptable. Further, let m stands for the mass of the load, g for the gravitational acceleration, $\phi(t)$ for the swing angle and $l(t)$ for the cable length. Using all these prerequisites, standard modelling gives the following nonlinear second order ordinary differential equations (ODE)

$$ml(t)\ddot{\phi}(t) + 2m\dot{l}(t)\dot{\phi}(t) + mg\sin\phi(t) = 0, \tag{1}$$

$$m\ddot{l}(t) - ml(t)\dot{\phi}^2(t) - mg\cos\phi(t) + \kappa\dot{l}(t) + F(t) = 0, \tag{2}$$

$$\phi \in (-\pi/2, \pi/2) \text{ and } l > 0, \tag{3}$$

where the ODE domain (3) is due to the obvious observation that $|\phi| > \pi/2$ would cause, at least initially, free fall of the mass rather than the pendulum like movement, while the string length is always positive. To apply control-theoretic methods, the second order ODEs should be converted into a first-order state space model. Three different state-space representations will be considered here.

To start with, [24] and the references therein use the following representation

$$\dot{x}_1 = x_2, \quad \dot{x}_2 = -x_3^{-1}(2x_2u + g\sin x_1), \quad \dot{x}_3 = u, \tag{4}$$

$$x_1 := \phi, \ x_2 := \dot{\phi}, \ x_3 := l, \ u := \dot{l}. \tag{5}$$

Note that the velocity of the string length variation dl/dt is considered to be controlled input. Denoting $x = (x_1, x_2, x_3)^\top$, the working equilibrium of (4) is $x^{eq} = (0, 0, l_0)^\top$, where l_0 is some desired nominal length of the string. Straightforward computations show that the approximate linearization of (4) around x^{eq} and $u = 0$ is

$$\dot{\xi} = \begin{bmatrix} 0 & 1 & 0 \\ -g/l_0 & 0 & 0 \\ 0 & 0 & 0 \end{bmatrix} \xi + \begin{bmatrix} 0 \\ 0 \\ 1 \end{bmatrix} u, \quad \xi := x - x^{eq},$$

which is neither controllable, nor stabilizable. Yet, (4) was asymptotically stabilized by a smooth feedback in [24,25].

Next, consider the following two-dimensional state space model

$$\dot{z}_1 = z_2\tilde{u}^{-2}, \ \dot{z}_2 = -g\tilde{u}\sin z_1, \quad z_1 := \phi, \ z_2 := \mathcal{I} = l^2\dot{\phi}, \ \tilde{u} := l. \tag{6}$$

As a matter of fact, model (6) considers the pendulum length as controlled input $\tilde{u} = l$, while the state $z_2 = \mathcal{I}$ is the angular momentum per unit mass with respect to the suspension point and the state $z_1 = \phi$ is the pendulum angle again. The second equation in (6) gives $(\mathrm{d}/\mathrm{d}t)(mz_2) = -mgl\sin z_1$, *i.e.,* the time derivative of the angular momentum with respect to the suspension point equals the torque created by the gravitational force momentum, hence, it is not changed by an instantaneous re-positioning of the mass. This will be useful in Section 3.2, where we consider a control strategy that varies the suspension length between two extreme positions in a bang-bang fashion. This would lead to an impulsive input signal and discontinuous state trajectories in the representation (4)-(5) while in (6), the respective state trajectories are continuous. To compare (6) and (4)-(5), note that for all $x_1 \in \mathbb{R}, x_2 \in \mathbb{R}, x_3 > 0$ diffeomorphism

$$z_1 = x_1, \ z_2 = x_2x_3^2, \ z_3 = x_3, \qquad x_1 = z_1, \ x_2 = z_2z_3^{-2}, \ x_3 = z_3, \tag{7}$$

transforms (4)-(5) into the following form

$$\dot{z}_1 = z_2z_3^{-2}, \quad \dot{z}_2 = -gz_3\sin z_1, \quad \dot{z}_3 = u. \tag{8}$$

In other words, (8) is obtained by "adding (an) integrator" to (6), *i.e.,* introducing the additional state variable z_3 and introducing the input $\tilde{u} = z_3$. This procedure can be also control-theoretically interpreted as mounting a simple dynamical feedback pre-compensator into the input channel.

Finally, consider the following four-dimensional state-space representation

$$\dot{x}_1 = x_2, \ \dot{x}_2 = -x_3^{-1}(2x_2x_4 + g\sin x_1), \ \dot{x}_3 = x_4, \ \dot{x}_4 = \overline{u}, \tag{9}$$

$$x_1 := \phi(t), \ x_2 := \dot{\phi}, \ x_3 := l, \ x_4 := \dot{l}, \tag{10}$$

$$\overline{u} = \ddot{l} = l\dot{\phi}^2 + g\cos\phi - (\kappa/m)\dot{l} - F/m. \tag{11}$$

Here, (11) is due to previously ignored (2) and (9) can be interpreted as "adding (an) integrator" to (4). Using notation $z_4 = x_4$ and (7), model (9) becomes

$$\dot{z}_1 = z_2 z_3^{-2}, \quad \dot{z}_2 = -g z_3 \sin z_1, \quad \dot{z}_3 = z_4, \quad \dot{z}_4 = \overline{u}, \tag{12}$$

thereby nicely relating all three models (6), (8) and (12). Note, that (11) is an easily implementable feedback transformation from the (in reality) controlled force $F(t)$ to the virtual input $\overline{u}$ to be used during the theoretical analysis. Indeed, knowing any state feedback controller for $\overline{u}$, one can easily implement the corresponding controller for $F(t)$ using (11). Note, that the common feature of all above models is the lack of stabilizability of the linearization around the origin.

2.2. Time-delay based control approach

In this short subsection, the control law of [19] is repeated for the reader's convenience. In the first place, this method motivates the research presented in Section 3. Secondly, it is used as comparison with newly proposed methods in Section 5. In [19] the open loop control rule

$$l(t) = l_0 - \Delta l \sin 2\Omega t, \tag{13}$$

originally proposed in [15], is transformed, by applying trigonometric identities, to the feedback control rule

$$l(t) = l_0 - \Delta l \frac{\phi^2(t-\tau_2) - e^{-\xi\pi}\phi^2(t-\tau_2-\tau_1)}{\phi^2(t-\tau_2) + e^{-\xi\pi}\phi^2(t-\tau_2-\tau_1)}. \tag{14}$$

Here, $\tau_1 = \frac{\pi}{2\Omega}$ and $\tau_2 = \frac{\pi}{4\Omega}$, with $\Omega = \sqrt{g/l_0}$ being the nominal natural oscillation frequency. The length adjustment amplitude Δl from the nominal pendulum length l_0 is given by

$$\Delta l = \frac{4}{3}\xi l_0. \tag{15}$$

With these parameters, the asymptotic behavior of an ideal second order damped oscillator is imposed, namely

$$\ddot{\phi}(t) + 2\xi\Omega\dot{\phi}(t) + \Omega^2\phi(t) = 0. \tag{16}$$

with ξ being the predefined desired damping.

Interestingly, as demonstrated by simulations and experiments in [19], control rule (13) and its feedback-based implementation (14) force the highly nonlinear system to behave as the linear oscillator in (16) even for relatively strong damping. Let us note that [15] also studied a saw-tooth discontinuous sliding motion. A considerable drawback of feedback rule (14) is that it varies the suspension length with a constant amplitude Δl even when $\phi \to 0$. As a consequence, for small ϕ, measurement and processes noise can induce closed loop instability.

2.3. Lyapunov based control design

For the reader's convenience, we also summarize our preliminary results, reported in [24] for state-space model (4). The experimental results of [24] will be compared later on with the results of the current paper. In order to asymptotically stabilize (4), the well-known control Lyapunov function (CLF) framework was used along with LaSalle type conditions. As an interesting feature, a repeated time differentiation of the respective equalities along the

solutions of (4) was needed to study the invariance of a certain set (as usual when applying LaSalle principle). More specifically, consider the Lyapunov function candidate V:

$$V(x_1, x_2, x_3) = gx_3(1 - \cos x_1) + \frac{x_3^2 x_2^2}{2} + c_1 \frac{(x_3 - l_0)^2}{2}, \tag{17}$$

with $c_1 > 0$. Note, that a Lyapunov-like function consisting of the first two terms in (17) was used in [22] and [23]. These references used, however, only the two dimensional model, and relied on some *ad hoc* way to change the suspension length x_3 without considering it as a state variable. So, another novelty of (17) consists of introducing the "penalty" term $c_1(x_3 - l_0)^2/2$ that forces the control law to keep the suspension length close to the prescribed length l_0 and that makes sure that x_3 eventually converges to l_0. By (17):

$$\frac{\mathrm{d}[V(x(t))]}{\mathrm{d}t} = \big(g(1 - \cos x_1) - x_3 x_2^2 + c_1(x_3 - l_0)\big)u. \tag{18}$$

Equality (18) suggests the following stabilizing feedback $u(x)$:

$$u(x) = -K\big(g(1 - \cos x_1) - x_3 x_2^2 + c_1(x_3 - l_0)\big), \tag{19}$$

where $K > 0$ and $c_1 > 0$ are design parameters, giving the following proposition.

Proposition 2.1 [24]**.** Consider system (4) in the region $\mathcal{D} = (-\pi/2, \pi/2) \times \mathbb{R} \times (0, \infty)$. Then $\forall K > 0$, $\forall c_1 > 0$ the control law given by (19) asymptotically stabilizes the equilibrium $(0, 0, l_0)$ of the system (4) with the region of attraction being the largest subset of $\mathcal{D}$ which is invariant with respect to trajectories of (4) and (19).

Remark 2.2. The region of attraction in Proposition 2.1 is not so easy to describe analytically, but it is practically reasonable. Obviously, it can be determined numerically and some limits on the initial velocity $x_2(0)$, depending on initial angle x_1, would be required not to overshoot the maximal allowed angle range $\pm\pi/2$. Besides, the condition $x_3 > 0$ might be easily achieved by choosing a sufficiently large c_1. Nevertheless, in practical applications one has to look for a much smaller region where trajectories evolve, *i.e.,* one has to look for control parameters c_1 and K that ensure much smaller limits for the angle x_1 than $\pm\pi/2$ and, in addition, x_3 should stay close to its desired length l_0 during the experiments. So, finding the largest invariant subset of $\mathcal{D} = (-\pi/2, \pi/2) \times \mathbb{R} \times (0, \infty)$ is mainly of theoretical interest.

2.4. Control feedback implementation

Assuming the overall system in the form (1)-(2), the so far presented control rules, including (14) and (19), provide only a partial solution. Notice that the input of the overall system (1)-(2) is the force F. Therefore, a slave (PD) control loop needs to be included to adjust the cable length l as shown in Fig. 2. Note that the master nonlinear controller *NCL* generates the set-point l_s for the cable length l which needs to be *almost ideally* tracked. This imposes enhanced performance requirements on the slave control loop. As demonstrated in [19] and [24], this task is difficult to achieve and requires further modification of the feedback loops, e.g. adjustment of the nominal delay in [19] or lag compensatoin in [24].

In order to avoid this additional tuning step, the second main goal of this paper is to design a nonlinear controller *NCF* for the scheme in Fig. 3, which directly generates the force F. This problem is solved in Section 4.

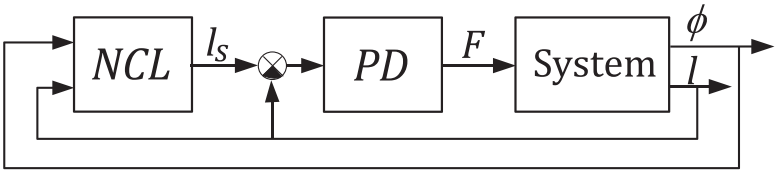

Fig. 2. Control scheme for implementing the control algorithm for (1)-(2) with l (its set-point l_s, respectively) being the control input.

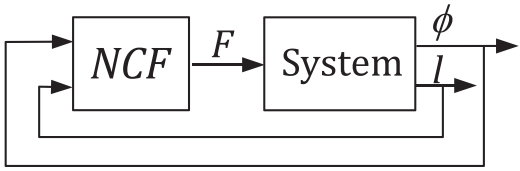

Fig. 3. Control scheme for implementing the control algorithm for (1)-(2) with F being the control input.

3. Theoretical limits and smoothed optimal solution

To get an intuition for a good control strategy, we will first study a conveniently formulated optimal control problem where only hard limits for the suspension length are imposed. The resulting control approach consists of varying the suspension length between its extremal values in a bang-bang fashion. Although this control approach is unrealistic in practice as it requires the suspension length to be changed infinitely fast, it serves as a good basis to shed light on the limitations of achievable damping. A feedback law obtained by smoothing of this discontinuous string length behaviour is proposed subsequently. This control law depends on a certain "trade-off" parameter between the steepness of string length changes and the damping intensity. A rigorous convergence proof of this last method concludes this section.

3.1. Numerical optimization based open loop control

To proceed with the above plan, we first compute an approximate solution to the following *open loop* optimal control problem based on state-space model (4):

$$\begin{gathered}\min_u \int_0^T \left(x_1^2(t)+x_2^2(t)\right)dt+\rho\left(x_1^2(T)+x_2^2(T)\right)\\ \text{such that (4) holds and}\\ |x_3(t)-l_0|\le 0.15\,l_0 \quad \forall t\in[0,+\infty), \quad x_1(0)=\pi/2,\ x_2(0)=0,\ x_3(0)=l_0,\end{gathered} \tag{20}$$

with the control horizon $T=20$, unit weight, a chosen weighting parameter $\rho=40$ and the desired length $l_0=1$. To compute an approximate solution for this optimization problem, a discretize-first approach is taken. States and controls are discretized with time-step $h=1/15$ and the cost function is discretized accordingly. A Runge-Kutta method of order four is used to approximate the system dynamics. This results in a nonlinear programming problem, with variables being the discretized states and controls, and constraints being the discretized dynamics and constraints, which can be solved in Matlab. Fig. 4 plots the obtained solution in the time interval [0, 10].

The resulting trajectory for the suspension length approximates a bang-bang signal, quickly changing between its extreme values. As a consequence, the input signal ($u=\dot{l}$) is close to

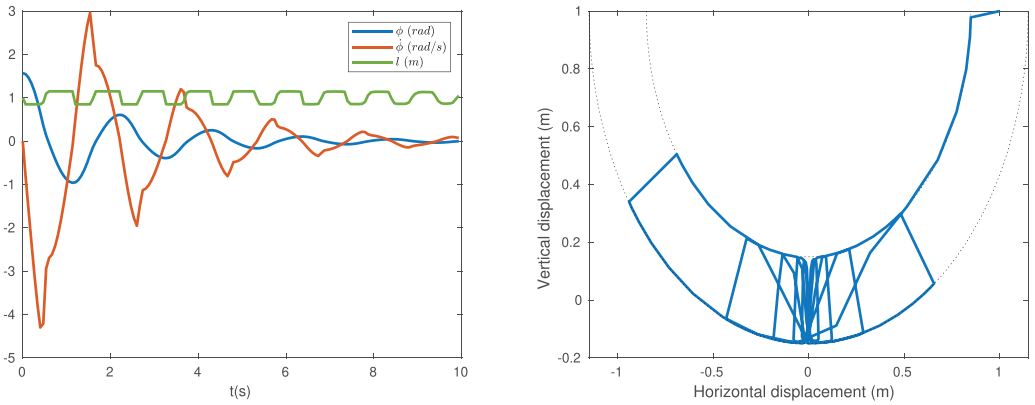

Fig. 4. Simulations of the optimal control in the sense of (20) with state space model (4). Left: the time evolution of the pendulum's angle (blue), its angular velocity (red) and the suspension length (green). Right: the Carthesian trajectory of the mass. (For interpretation of the references to colour in this figure legend, the reader is referred to the web version of this article.)

impulsive, resulting in an almost discontinuous trajectory for $x_2 = \dot{\phi}$. Note that the period of the suspension length's trajectory is equal to half the period of the angle's trajectory. Moreover, the resulting trajectories are close to those presented in Fig. 8 of [15], which are based on estimating the damping ratio during the saw-tooth-like approximation of the bang-bang length variation. Finally, the persistently varying nature of the length trajectory compensates the non-controllability of the linearization at the equilibrium to be reached.

3.2. Analysis of the limit case

In this subsection, the above suggested limit case is analysed. Namely, let the suspension length be subject to a switched bang-bang control law:

$$l(t) = \begin{cases} l_0 - \Delta l & \text{if} \dot{\phi}(t) \sin \phi(t) < 0, \\ l_0 + \Delta l & \text{if} \dot{\phi}(t) \sin \phi(t) \geq 0, \end{cases} \tag{21}$$

with $0 < \Delta l < l_0$. This control law will extend the pendulum instantaneously at zero angle to its maximum length $l + \Delta l$ and shorten it instantaneously at zero angular velocity to its minimal length $l - \Delta l$.

In the coordinates of (4) control law (21) behaves as an impulsive input since $u = \dot{l}$ and introduces state-jumps in $x_2 = \dot{\phi}$ and $x_3 = l$. A natural way to handle state-jumps induced by impulsive forces consists of using a hybrid system representation, with both continuous and discrete dynamics, see e.g. [35] and the references therein:

$$\begin{cases} \dot{x}(t) = F(x(t)), x \in C, \\ x+ = G(x), x \in D, \end{cases} \tag{22}$$

where C is the so-called *flow set* and D the *jump set*. For control law (21):

$$D = \bigcup_{i=1}^{3} D_i, \quad C = \mathbb{R}^3 \setminus D,$$

$$D_1 = \{x \in \mathbb{R}^3 : \ x_1 = 0, \ x_3 = l_0 - \Delta l\}$$
$$D_2 = \{x \in \mathbb{R}^3 : \ x_2 = 0, \ x_3 = l_0 + \Delta l\}$$
$$D_3 = \{x \in \mathbb{R}^3 : \ x_3 \notin \{l_0 - \Delta l, l_0 + \Delta l\}\}.$$

The continuous dynamics in (22) can be spelled out as follows:

$$\dot{x}_1(t) = x_2(t), \quad \dot{x}_2(t) = -\frac{g}{x_3(t)} \sin x_1(t), \quad \dot{x}_3(t) = 0, \tag{23}$$

while the jump map in (22) is described by

$$G(x) = \begin{cases} (x_1, \ \alpha x_2, \ l_0 + \Delta l), & x \in D_1, \\ (x_1, \ \beta x_2, \ l_0 - \Delta l), & x \in D_2, \\ (x_1, \ \beta x_2, \ l_0 - \Delta l), & x \in D_3, \end{cases}$$

$$\alpha = \left(\frac{l_0 - \Delta l}{l_0 + \Delta l}\right)^2, \ \beta = \left(\frac{x_3}{l_0 - \Delta l}\right)^2. \tag{24}$$

The continuous dynamics describe the pendulum's movement for a fixed length, *i.e.,* an undamped pendulum. The constants (24), determining the jump map, directly follow from the *preservation of angular momentum* for the full extension and retraction

$$\big(m \ (l_0 + \Delta l)^2\big)x_2+ = \big(m \ (l_0 - \Delta l)^2\big)x_2, \quad \big(m \ (l_0 - \Delta l)^2\big)x_2+ = \big(m \ {x_3}^2\big)x_2, \tag{25}$$

respectively, as the gravity does not impose an impulsive torque.

Remark 3.1. A hybrid system description of the form (22), with variables x_1 and x_2 only, is not possible. Encoding the logic $x_1 = 0 \ \Rightarrow \ x_2+ = \alpha x_2$ in the definition of D and G would lead to infinitely many consecutive jumps because $x_2 \in D$ would imply $x_2+ \in D$. This is resolved by introducing x_3 as a real valued variable. Its values different from $l_0 \pm \Delta l$, which are non relevant for the control strategy, are handled by jump subset D_3. For all t strictly larger than the initial time, variable x_3 thus only takes two discrete values.

Remark 3.2. Hybrid system (22)–(24) does not have an asymptotically stable equilibrium, as only the "projected" state (x_1, x_2) converges to zero.

When considering the (x_1, x_2)-subspace, the effect of the state-jumps is two-fold. Firstly, they lead to a switching of the continuous dynamics (23) (induced by changing the pendulum's length x_3). Secondly, they cause a jump in the angular velocity x_2. This leads us to the following interpretation:

A. When ignoring the jump in the angular velocity, *i.e.* using $\alpha = 1$ in (24), the system can be interpreted as a *switched system* on $\mathbb{R}^2$:

$$\dot{x}_1(t) = x_2(t), \ \dot{x}_2(t) = -\frac{g}{l(t)} \sin x_1(t), \ l(t) = l_0 + \Delta l \operatorname{sign}\big[x_2(t) \sin(x_1(t))\big]. \tag{26}$$

The equilibrium $x_1 = x_2 = 0$ of the switched system is *unstable*. Indeed, for any initial state $(0, x_{2,\text{out}})$ with arbitrarily small $|x_{2,\text{out}}| \in \mathbb{R}$ the pendulum will swing up till a maximum angle $x_{1,m}$ given by $(1/2)m((l_0 + \Delta l)x_{2,\text{out}})^2 = mg(l_0 + \Delta l)(1 - \cos(x_{1,m}))$. Then it will return to $x_1 = 0$ with angular velocity $x_{2,\text{in}}$ given by $mg(l_0 - \Delta l)(1 - \cos(x_{1,m})) = m((l_0 - \Delta l) \ x_{2,\text{in}})^2/2$. These relations imply that $x_{2,\text{in}} = \gamma \ x_{2,\text{out}}$, with

$$\gamma = (l_0 + \Delta l)^{\frac{1}{2}} (l_0 - \Delta l)^{-\frac{1}{2}} > 1. \tag{27}$$

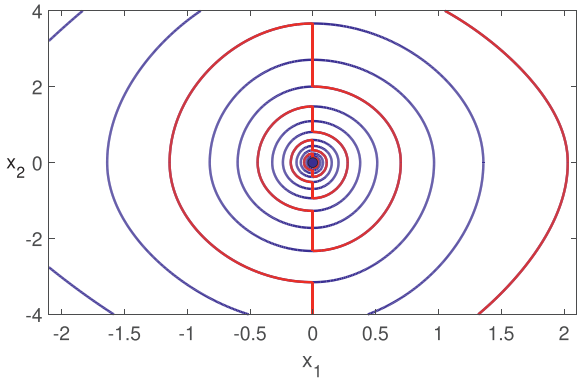

Fig. 5. Blue curve - trajectory of (26) for $l_0 = 1$ and $\Delta l = 0.15$ (length switching between 0.85 and 1.15). As a function of time, the state variables move in clockwise direction along the trajectory. Red curve - projection of trajectory of (22)–(24) on the (x_1, x_2)-plane.

Hence, system (26) is an example of the well known phenomenon, where instability is induced by "unfortunate" switching between two (in this case marginally) stable systems. In Fig. 5 the blue curve shows a trajectory of (26).

B. When the jump in angular velocity at $x_1 = 0$ is taken into account, *i.e.,* parameter α as in (24), the projected dynamics on the (x_1, x_2)-plane become asymptotically stable. This is because the increase in angular velocity with factor (27) per half period of the continuous phase is over-compensated by the velocity reduction at the jumps with a factor $\alpha = -\gamma^{-4}$. Hence, the effect of the velocity jump can be interpreted as the effect of *moving two periods back in time* along the solution of (26). This property is visualized in Fig. 5 (red curve).

In terms of the coordinates in (6), control law (21) does not give rise to discontinuous state trajectories, as the instantaneous re-positioning of the mass does not change the angular momentum. The resulting closed-loop system is a switched system in $\mathbb{R}^2$:

$$\begin{aligned} \dot{z}_1(t) &= l(t)^{-2} z_2(t), \quad \dot{z}_2(t) = -l(t) g \sin z_1(t), \\ l(t) &= l_0 + \Delta l \operatorname{sign}\big[z_2(t) \sin(z_1(t))\big]. \end{aligned} \tag{28}$$

Fig. 6 shows the trajectory of (28) corresponding to the red curve displayed in Fig. 5. Clearly the exponential stability is induced here by the proper switching between two otherwise undamped oscillators. It is interesting to note here that this situation very much resembles the analysis of a switched control law inducing stability in [34], where a bilinear second-order system is stabilized by switching between the vector fields of a marginally stable system and an unstable system. For stability and stabilization of switched systems the reader is referred to [36].

3.3. A smooth feedback law

This section studies the smooth feedback law $\tilde{u}(z)$ approximating the discontinuous feedback $\tilde{u}^{dsc}(z) := l(t)$, with $l(t)$ given in (21). For every value of the "smoothing" parameter $\epsilon > 0$: define

$$\widetilde{u}(z) := l_0 + \Theta_{\Delta l, \varepsilon}(z_2 \sin z_1), \tag{29}$$

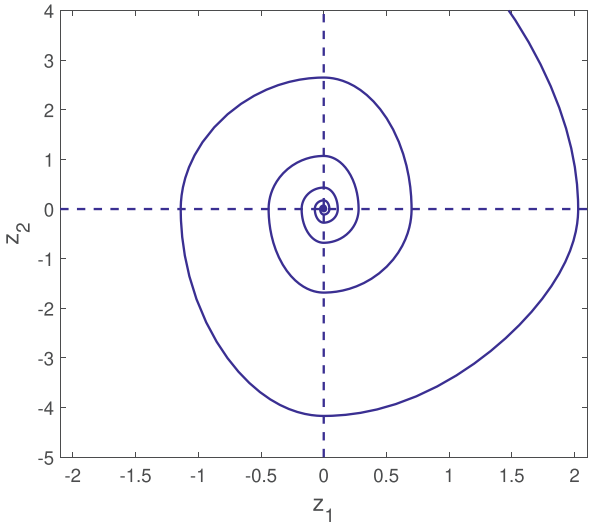

Fig. 6. Solution of (28). Stability is induced by switching between ellipsoidal curves, stretching in horizontal, respectively vertical direction.

in which $\Theta_{\Delta l,\varepsilon}(x) : \mathbb{R} \mapsto [\Delta l, -\Delta l]$ is defined $\forall x \in \mathbb{R}$ as

$$\Theta_{\Delta l,\varepsilon}(x) = \begin{cases} -\Delta l & \text{if } x \le -\varepsilon, \\ -\Delta l \; e^{\frac{1}{x}}\left(e^{\frac{1}{\varepsilon}} - e^{\frac{1}{-x-\varepsilon}}\right) & \text{if } x \in (-\varepsilon, 0), \\ 0 & \text{if } x = 0, \\ \Delta l \; e^{-\frac{1}{x}}\left(e^{\frac{1}{\varepsilon}} - e^{\frac{1}{x-\varepsilon}}\right) & \text{if } x \in (0, \varepsilon), \\ \Delta l & \text{if } x \ge \varepsilon. \end{cases} \tag{30}$$

Function (30) serves as a smooth ε-approximations of the sign function in (28). Indeed, one can compute derivatives of any order of the function $\Theta_{\Delta l,\varepsilon}(x)$ and then show their continuity at critical points $\pm\varepsilon$, 0 by virtue of the well-known limit

$$\lim_{x \to 0-} x^{-k} e^{\frac{1}{x}} = 0, \;\; \forall k \ge 0.$$

Fig. 7 shows $\Theta_{\Delta l,\varepsilon}(x)$ for several values of ε. It is clear that $\Theta_{\Delta l,\varepsilon}(x)$ approximates a step function as ε goes to zero.

Theorem 3.3. *Let any pair $(l_0, \Delta l)$ satisfying $0 < \Delta l < l_0$ be given. Then, for all $\epsilon > 0$, the smooth control law (29) asymptotically stabilizes (6) at the origin. The inner estimate of the respective basin of attraction is*

$$\mathcal{A} = \{z \in \mathbb{R}^2 | \, z_2^2 < 2gl_0^3 \cos z_1 \;\; \wedge \;\; z_1 \in (-\pi/2, -\pi/2)\}.$$

Proof. Consider the Lyapunov function $\widetilde{V}(z) = gl_0^3(1 - \cos z_1) + z_2^2/2$. The set $\mathcal{A}$ consists of points z for which $\widetilde{V}(z(t)) < \widetilde{V}((\pi/2, 0)^\top)$ and $z_1 \in (-\pi/2, -\pi/2)$. Straightforward computations of the derivative of $\widetilde{V}$ along the solutions of the closed-loop system yield

$$\dot{\widetilde{V}} = gz_2 \sin z_1 (l_0^3 \widetilde{u}^{-2}(z) - \widetilde{u}(z)) = \widetilde{u}^{-2}(z) g z_2 \sin z_1 (l_0^3 - \widetilde{u}^3(z)),$$

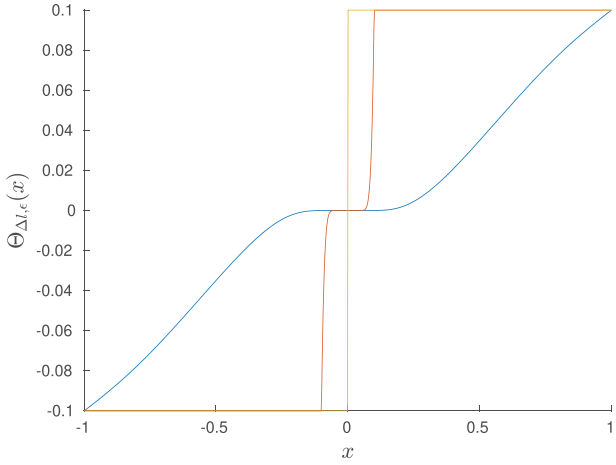

Fig. 7. $\Theta_{\Delta l,\varepsilon}(x)$ on the interval $[-1, 1]$ for $\Delta l = 0.1$ and ε equal to 1 (blue), 0.1 (red) and 0.0001 (yellow). (For interpretation of the references to colour in this figure legend, the reader is referred to the web version of this article.)

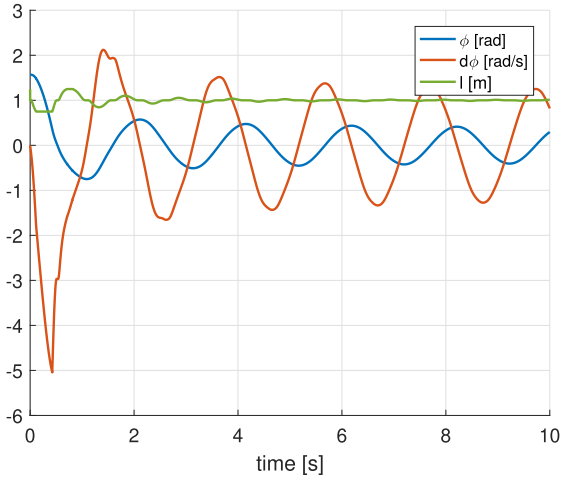

Fig. 8. Simulations: the time evolution of the pendulum's angle (blue), the angular velocity (red) and the pendulum length (green) - the smoothed feedback (29) with parameter $\epsilon = 1$. (For interpretation of the references to colour in this figure legend, the reader is referred to the web version of this article.)

with control law $\widetilde{u}(z)$ defined by (29). Moreover, it holds that

$$\widetilde{u}(z)\begin{cases} < l_0 \text{ for } z_2 \sin z_1 < 0, \\ = l_0 \text{ for } z_2 \sin z_1 = 0, \\ > l_0 \text{ for } z_2 \sin z_1 > 0. \end{cases}$$

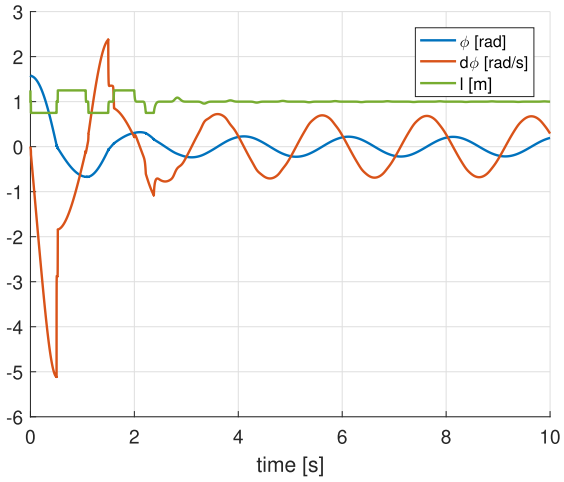

Fig. 9. Simulations: the time evolution of the pendulum's angle (blue), the angular velocity (red) and the pendulum length (green) - the smoothed feedback (29) with parameter $\epsilon = 0.1$. (For interpretation of the references to colour in this figure legend, the reader is referred to the web version of this article.)

From $\text{sign}(l_0^3 - \widetilde{u}^3) = \text{sign}(l_0 - \widetilde{u})$, it follows that

$$l_0^3 - \widetilde{u}^3(z) \begin{cases} >0 \text{ for } z_2 \sin z_1 < 0, \\ = 0 \text{ for } z_2 \sin z_1 = 0, \\ < 0 \text{ for } z_2 \sin z_1 > 0. \end{cases}$$

As a consequence, it obviously holds for all $z \in \mathcal{A}$ that

$$\dot{\widetilde{V}} < 0 \ \forall z_1 \neq 0 \wedge z_2 \neq 0, \tag{31}$$

and $\dot{\widetilde{V}} = 0$ elsewhere. Now, asymptotic stability can be concluded using standard LaSalle theorem arguments, since the largest invariant subset of the set where $z_1 = 0$ or $z_2 = 0$ is the origin and therefore $z(t) \to 0$ as $t \to \infty$. The mentioned invariant property can be easily deduced from (6) since $\dot{z}_1 = 0$ implies $z_2 = 0$ and $\dot{z}_2 = 0$ implies $z_1 = 0$. □

The performance of this smooth feedback law is demonstrated in simulations in Figs. 8, 9 and 10 for various ε. Note that the simulations are performed in z-coordinates, but then the real angular velocity is computed from $z_2(t)$ knowing the current value of $l(t)$. These simulations nicely and convincingly show that by reducing ϵ the improvement of the convergence rate and the aggressiveness of the controller go hand-in-hand. They also show that one may use larger ε at the beginning and only later switch to smaller value, thereby achieving good convergence with a less aggressive control action. Note that the simulations charts were cut at time equal to 10 sec. since later on the damping proceeds very slowly (almost no control action). Moreover, one can see that the initial damping phase is almost the same for all ε. Note also that for small amplitudes, even $\varepsilon = 0.001$, an aggressive controller action is not required. The reason is that then the pendulum behaves like a linear one, *i.e.* each cycle takes the same time regardless how small the amplitude is. In such a way, the passage through the sharp region of the smoothing function Θ is slower and slower, and the controller is acceptable from a practical point of view.

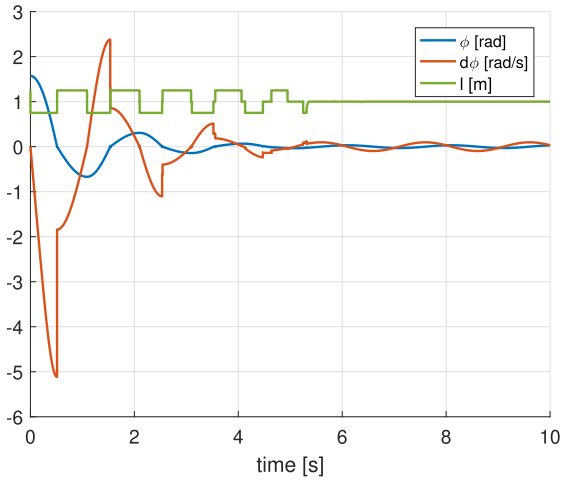

Fig. 10. Simulations: the time evolution of the pendulum's angle (blue), the angular velocity (red) and the pendulum length (green) - the smoothed feedback (29) with parameter $\epsilon = 0.001$. (For interpretation of the references to colour in this figure legend, the reader is referred to the web version of this article.)

4. Using the force as the control input

As mentioned in Subsection 2.4, in all the previous approaches, the dynamics of the suspension length, as given in (2), have been ignored, basically considering l or $\dot{l}$ to be the input in (1). Thus, a slave control loop was needed to implement such control laws, as shown in Fig. 2. In this section a more practical setting where the suspension length is dictated by (2), will be considered. As a starting point, the feedback controller (19) stated in Proposition 2.1 for the three dimensional state space model (4) is taken. Subsequently, a backstepping procedure [37] is used to introduce a feedback law for (9)-(11). Further, more sophisticated results on backstepping and stabilization when smooth feedback is not available can be found in [38–41]. The backstepping procedure can be viewed as a rigorously justified model based version of the PD block shown in Fig. 2. Indeed, all information contained in the block NCL (the asymptotically stabilizing feedback (19) for system (4) and the respective Lyapunov function (17)) will be used to generate the overall block NCF in Fig. 3.

The proof of the asymptotic stability of the resulting closed loop system will require additional and rather non-trivial LaSalle invariance principle based analysis as well.

To proceed with the above idea, the backstepping procedure introduces the Lyapunov function candidate $\overline{V}$ for (9) as

$$\overline{V} = V + \frac{(x_4 - u(x))^2}{2}, \tag{32}$$

where $u(x)$ is given by (19) and it is by Proposition 2.1 the asymptotically stabilizing feedback for the system (4). Moreover, V given by (17) is the Lyapunov function justifying that stability. Plugging the expressions for u and V into (32), we obtain (recall that $K > 0$, $c_1 > 0$):

$$\overline{V} = gx_3(1 - \cos x_1) + \frac{x_3^2 x_2^2}{2} + c_1\frac{(x_3 - l_0)^2}{2} + \frac{\big(x_4 + K\big(g(1 - \cos x_1) - x_3x_2^2 + c_1(x_3 - l_0)\big)\big)^2}{2}. \tag{33}$$

Further computations give rise to the full time derivative of $\overline{V}$ along a trajectory $x(t)$ of (9):

$$\begin{aligned}\dot{\overline{V}} :&= \frac{\mathrm{d}[\overline{V}(x(t))]}{\mathrm{d}t} = gx_3(\sin x_1)x_2 - \frac{x_3^2x_2}{x_3}g\sin x_1\\ &+\left(g(1-\cos x_1)+x_3x_2^2-2x_3^2x_2\frac{1}{x_3}x_2+c_1(x_3-l_0)\right)x_4\\ &+\big(x_4+K\big(g(1-\cos x_1)-x_3x_2^2+c_1(x_3-l_0)\big)\big)\\ &\times\left(\overline{u}+K\frac{\mathrm{d}}{\mathrm{d}t}\big(g(1-\cos x_1)-x_3x_2^2+c_1(x_3-l_0)\big)\right),\end{aligned}$$

$$\begin{aligned}\dot{\overline{V}} &= \big(g(1-\cos x_1)-x_3x_2^2+c_1(x_3-l_0)\big)x_4+\big(x_4+K\big(g(1-\cos x_1)-x_3x_2^2+c_1(x_3-l_0)\big)\big)\\ &\times\big(\overline{u}+K\big(gx_2\sin x_1-x_4x_2^2+2x_2(2x_2x_4+g\sin x_1)+c_1x_4\big)\big).\end{aligned}\tag{34}$$

Referring to (19) one can state more compactly that

$$\dot{\overline{V}} = \frac{-u(x)x_4}{K}+(x_4-u(x))\left(\overline{u}-\frac{\mathrm{d}u(x)}{\mathrm{d}x}\frac{\mathrm{d}x}{\mathrm{d}t}\right).\tag{35}$$

Next, observe that (35) can be adapted as follows

$$\dot{\overline{V}} = \frac{-u(x)^2}{K}-\frac{u(x)(x_4-u(x))}{K}+(x_4-u(x))\left(\overline{u}-\frac{\mathrm{d}u(x)}{\mathrm{d}x}\frac{\mathrm{d}x}{\mathrm{d}t}\right).$$

Next, define the following feedback $\overline{u}$

$$\overline{u}(x) = \frac{u(x)}{K}+\frac{\mathrm{d}u(x)}{\mathrm{d}x}\frac{\mathrm{d}x}{\mathrm{d}t}-K_2(x_4-u(x)),\quad K,\ K_2>0.\tag{36}$$

Substituting to (36) from (19) one gets the following explicit formula for $\overline{u}(x)$

$$\begin{aligned}\overline{u}(x) &= -K\big(gx_2\sin x_1-x_4x_2^2+2x_2(2x_2x_4+g\sin x_1)+c_1x_4\big)\\ &-(K_2K+1)\big(g(1-\cos x_1)-x_3x_2^2+c_1(x_3-l_0)\big)\\ &-K_2x_4,\quad c_1>0,\ K>0,\ K_2>0.\end{aligned}\tag{37}$$

Using (36) gives

$$\dot{\overline{V}} = -K^{-1}u(x)^2-K_2(x_4-u(x))^2\le 0,\ \ K>0,K_2>0.\tag{38}$$

Note, that $\dot{\overline{V}}=0$ if and only if $u(x)=0\wedge x_4=0$. In the sequel of this subsection, we denote this set as $\overline{V}_{d,0}$. Next, we aim to show that the largest subset of $\overline{V}_{d,0}$ which is invariant with respect to trajectories of (9), (37) consists of the single point $(0,0,l_0,0)^\top$. Since $u(x)$ is given by (19), it holds that $g(1-\cos x_1)-x_3x_2^2+c_1(x_3-l_0)=u(x)=0,\ x_4=0,\quad \forall x\in\overline{V}_{d,0}$. Realize that the mentioned invariance means that the above equalities must hold along trajectories of (9), (37) and therefore time differentiation gives $gx_2\sin x_1-x_4x_2^2+2x_2x_3x_3^{-1}(2x_2x_4+g\sin x_1)+c_1x_4=0$. As already noted, $x_4=0$ for all $x\in\overline{V}_{d,0}$ and therefore this last equality gives $x_2\sin x_1=0$ for all $x\in\overline{V}_{d,0}$. Differentiating $x_2(t)\sin x_1(t)=0$ with respect to time along trajectories of (9), (37) and recalling again that $x_4=0$ for all $x\in\overline{V}_{d,0}$ one gets $-x_3^{-1}g\sin^2x_1+x_2^2\cos x_1=0$. Summarizing, we have shown that for every x

belonging to any subset of $\overline{V}_{d,0}$, invariant with respect to (9), (37), it holds that

$$x_4 = 0, \qquad g(1-\cos x_1) - x_3 x_2^2 + c_1(x_3 - l_0) = 0, \tag{39}$$

$$x_2 \sin x_1 = 0, \quad x_3^{-1} g \sin^2 x_1 - x_2^2 \cos x_1 = 0. \tag{40}$$

Since $x_1 \in (-\pi/2, \pi/2)$ and $x_3 > 0$ by the basic settings (3), (40) implies that $x_1 = x_2 = 0$. Indeed, by the first equality in (40) either $x_2 = 0$ or $\sin x_1 = 0$, *i.e.* $x_1 = 0$ by $x_1 \in [-\pi/2, \pi/2]$. Now, substituting $x_1 = 0$ into the second equality in (40) gives $x_2 = 0$ while substituting $x_2 = 0$ into the second equality in (40) gives $x_1 = 0$. Next, substituting $x_1 = x_2 = 0$ to the second equality in (39) gives for $c_1 > 0$ that $x_3 = l_0$. In such a way, together with already mentioned equality $x_4 = 0$, we have just demonstrated that the set $\{x = (0, 0, l_0, 0)^\top\}$ is the only subset of the set $\overline{V}_{d,0}$ that is invariant with respect to trajectories of (9) with $\overline{u}$ from (36)-(37).

Summarizing, for $\overline{V}(x)$ given by (32) with $\overline{V}((0, 0, l_0, 0)^\top) = 0$, $\overline{V}(x) > 0$, $\forall x \neq (0, 0, l_0, 0)^\top$ it holds by (38) that $\dot{\overline{V}} \leq 0$, $\forall x \neq (0, 0, l_0, 0)^\top$) and that $\{(0, 0, l_0, 0)^\top\}$ is the largest subset of $\{x \in \mathbb{R}^4 | \dot{\overline{V}} = 0\}$, invariant for (9), (36), (37). So, by virtue of the well-know LaSalle principle [37] we have just proven the following result.

Theorem 4.1. *Let $K > 0, K_2 > 0, c_1 > 0$ are given and denote $\mathcal{D} \times \mathbb{R}$, with $\mathcal{D} = (-\pi/2, \pi/2) \times \mathbb{R} \times (0, \infty)$. Then feedback law (37) asymptotically stabilizes system (9) at the equilibrium $(0, 0, l_0, 0)^\top$ with the region of attraction being the largest subset of $\mathcal{D} \times \mathbb{R}$ which is invariant with respect to trajectories of (9), (37).*

Theorem 4.2. *Similar comments as in Remark 2.2 obviously apply regarding the region of attraction mentioned in Theorem 4.1.*

Remark 4.3. In the real-life setup, however, the cable can only pull. This means that the control force F must always be non-negative. In the simulations and experiments that are presented in the next section, this was achieved by feeding the output of the control law to a saturation function which puts the cart force to zero when it becomes negative. More specifically, rewriting the definition (11) of $\overline{u}$ in terms of $x_1 := \phi$, $x_2 := \dot{\phi}$, $x_3 := l$, $x_4 := \dot{l}$, gives

$$\overline{u} = x_3 x_2^2 + g \cos x_1 - (\kappa/m) x_4 - F/m, \tag{41}$$

$$\overline{u} \leq x_3 x_2^2 + g \cos x_1 - (\kappa/m) x_4, \tag{42}$$

where the saturation (42) holds by $F \geq 0$. Note, that the virtual input $\overline{u}$ has a clear physical meaning being the second time derivative of the string length.

5. Simulations and experiments

5.1. Simulations

In this subsection, the newly developed, nonlinear feedback law in (37), designed by backstepping, is compared with the time delay feedback (14) of [19] and Lyapunov based feedback (19) of [24] using simulations. One of the important purposes of simulations of the newly developed controller (37) is to tune its positive parameters K, K_1, c_1. Note, that while K, K_1 are typical gain-like parameters to be tuned to achieve nice performance, the parameter

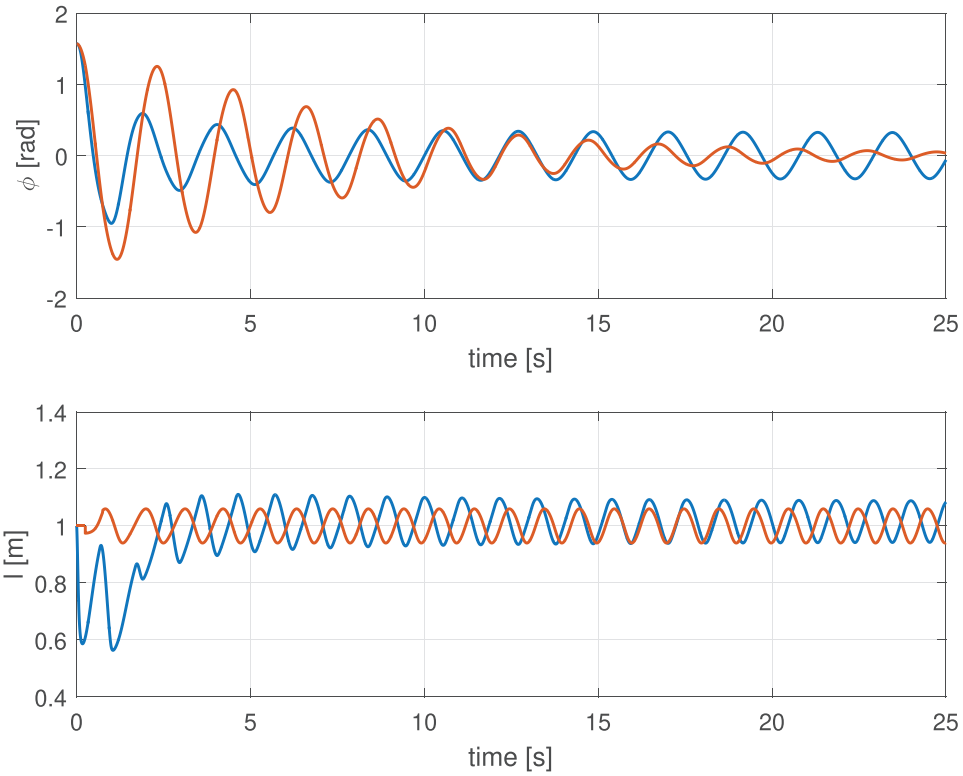

Fig. 11. Simulations: the time evolution of the pendulum angle and the pendulum length during the controlled swing. The blue line corresponds to the newly derived feedback (37), the red line to time delay feedback (14) of [19]. (For interpretation of the references to colour in this figure legend, the reader is referred to the web version of this article.)

c_1 determines the trade-off between controller aggressiveness and string length variation due to the CLF (33) term $c_1(x_3 - l_0)^2/2$ (recall $x_3 := l$).

Note that the feedback (37) is simulated on the full model (1)-(2), while (14) and (19) are simulated on the sub-model (1). The parameters of the model are given as $l_0 = 1\,[\mathrm{m}]$ and $m = 1\,[\mathrm{kg}]$. The friction is neglected here, i.e. $\kappa = 0\,[\mathrm{kg\,s^{-1}}]$.

The comparison is shown in Figs. 11 and 12, respectively. In the upper part of the figures, the trajectories of the pendulum angle are shown, whereas the evolution of the pendulum's length is shown in the bottom. In both the cases the suppression of the pendulum swing with initial deviation $\phi(0) = \frac{\pi}{2}\,[\mathrm{rad}]$ and the zero angular velocity $\dot{\phi}(0) = 0$ $\kappa = 0\,[\mathrm{rad\,s^{-1}}]$ was simulated over a 25 seconds horizon. The following controller parameters were considered: $K = 4$, $K_2 = 12.5$, $c_1 = 10$ for (37); $K = 0.25$, $c_1 = 10$ for (19); $\xi = 0.05$ resulting to $\Delta l = 0.067\,[\mathrm{m}]$ in (14).

The behavior of the trajectories reflects the theory presented in the previous sections. The pendulum swinging seems not to vanish completely using the Lyapunov-based controllers as the slow asymptotic decay is related to the lack of local exponential stability. The suppression efficiency of the approach based on the time-delay control law (14) in Fig. 11 can be attributed to the constant amplitude of the control signal, despite the decaying amplitude of the oscillation to be suppressed. Notice that even though the novel feedback (37) was tested

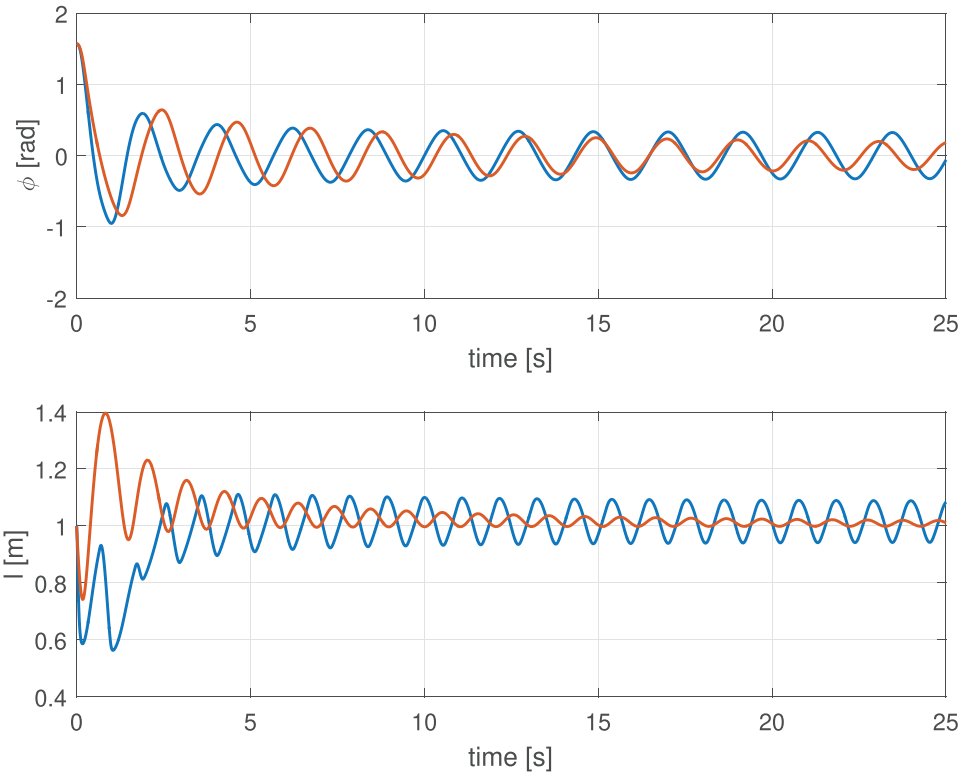

Fig. 12. Simulations: the time evolution of the pendulum angle and the pendulum length during the controlled swing. The blue line corresponds to the newly derived feedback (37), the red line to feedback (19) of [24]. (For interpretation of the references to colour in this figure legend, the reader is referred to the web version of this article.)

on a more complex model, analogous result has been achieved as for the simpler case with (19).

5.2. Experiments

In a second step, feedback law (37), proposed by backstepping, is compared experimentally with both the time delay feedback (14) and Lyapunov based feedback (19) on the setup shown in Fig. 13. Note that this setup was used already in [19] and [24]. It consists of an externally controlled movable cart connected with the suspended load via a cable of fixed length. As it can be seen in the detail of Fig. 13, the cable passes through a pulley at the fixed base and an arm of the rotational sensor which measures the pendulum angle. The cable length is controlled via the position of the movable cart which itself is driven by an actuator via a rotating belt. The actuator is controlled by an industrial control unit which operates in a torque regime, *i.e.,* the input of the industrial control unit is the reference torque to be generated by the actuator. The rotating belt transforms the torque generated by the actuator to the force applied to the movable cart. The cart position is measured using an incremental sensor.

For the purpose of the current research, the experimental setup presented in [19] and [24] was further enhanced. In particular, the industrial controller CompactRIO and Labview

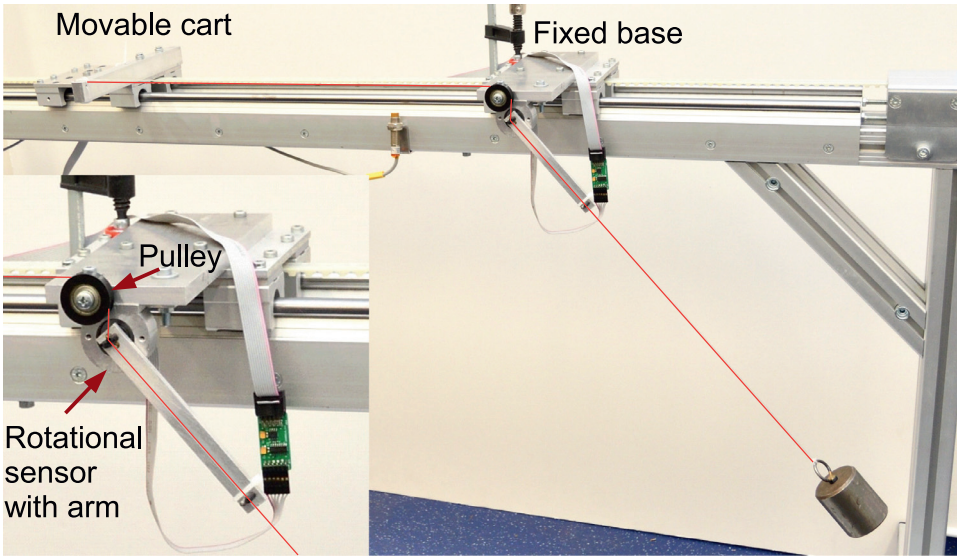

Fig. 13. The experimental setup for validation of the proposed methods.

substituted PC with measurement board and Matlab-Simulink used earlier. This brought a substantial improvement in reliability and computational efficiency, including the measurements by virtue of the FPGA and fast TTL input/output blocks.

For time-delay feedback (14) the input of the controller is the pendulum angular position ϕ and the output is the instantaneous required cable length l. To implement this output, a position PD controller was used to achieve the desired pendulum length by movement of the cart. For control law (19), the controller output $u(t)$ is the desired velocity of the pendulum cable $\dot{l}$. For this purpose, a linear velocity observer was developed and a velocity PD controller was designed and tuned to adjust the instantaneous desired velocity of the cable length via the velocity control of the movable cart. Thus, for these two control implementations, the scheme according to Fig. 2 was applied, supplemented by the velocity observer for the latter.

The implementation of the feedback (37) designed by backstepping was considerably easier, namely as $\bar{u}(t)$ represents the desired acceleration of the pendulum string $\ddot{l}(t)$, the desired force $F(t)$ can be determined from (11) as

$$F(t) = ml(t)\dot{\phi}^2(t) + mg\cos\phi(t) - \kappa\dot{l}(t) - m\bar{u}(t). \tag{43}$$

for which $(d\phi/dt)$ and (dl/dt)] are estimated by local observers. The advantage of generating the control force by (43) is also in compensation of viscous friction and the effects of the gravitational and centrifugal forces. Moreover, the control scheme (37), (2) is naturally robust with respect to an unknown viscous friction coefficient κ as (37) contains the term K_2x_4, $x_4 = (dl/dt)$ where $K_4 > 0$ is a tunable control gain. Finally, the control feedback implementation is according to the straightforward scheme in Fig. 3 supplemented by the local observers for the unmeasured angular velocity and the string length variation velocity.

The identified parameters of the set-up model according to (1)-(2) are $m = 0.8$ [kg] and $\kappa = 15$ [kg s^{-1}]. The nominal cable length $l_0 = 0.6$[m] was considered. The following controller parameters were applied: $K = 4$, $K_2 = 12.5$, $c_1 = 10$ for (37); $K = 0.5$, $c_1 = 10$ for (19);

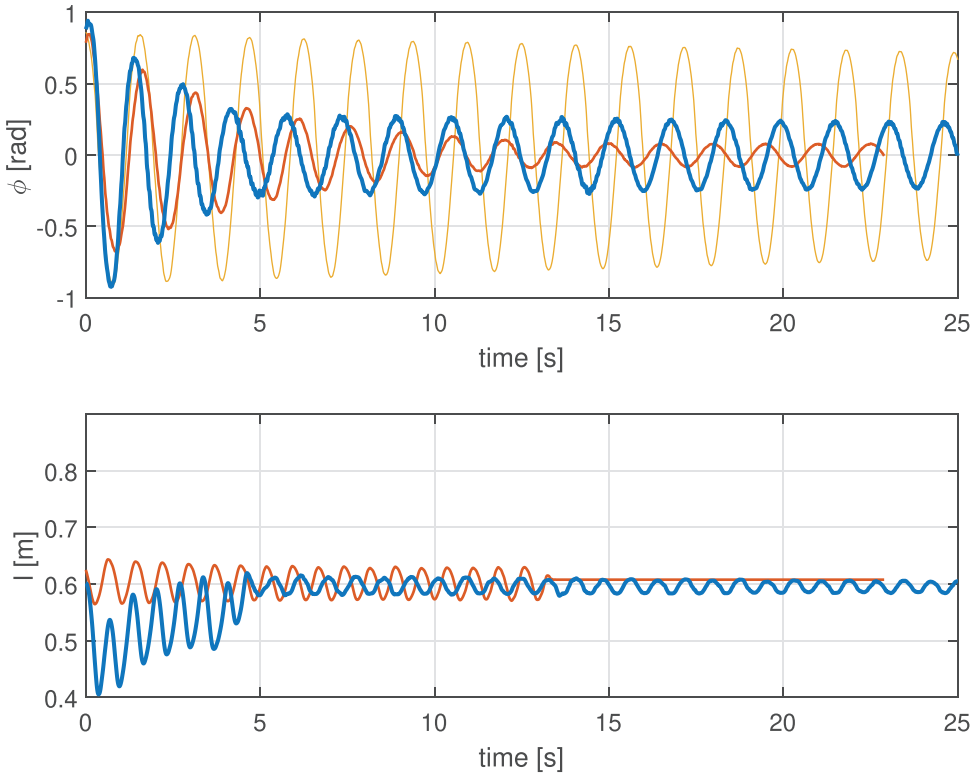

Fig. 14. Experiments: the time evolution of the pendulum angle and the pendulum length during the controlled swing. The blue line corresponds to the newly designed force controller (37), (43), the red line to the time delay feedback (14) and the yellow line to the uncontrolled swing. (For interpretation of the references to colour in this figure legend, the reader is referred to the web version of this article.)

$\xi = 0.05$ providing $\Delta l = 0.04$[m] for (14). The results of the performed experiments are shown in Figs. 14 and 15, respectively, where also the almost undamped pendulum swing with $l_0 = 0.6$[m] is shown for comparison. Analogously to simulations, the trajectories of the pendulum angle are shown in the upper part of the figures, whereas the pendulum length evolution during the swing damping is shown in the bottom. In all the experiments an initial angle of around 0.85 [rad] was used.

First, the proposed *control by force* feedback law (defined by (37) and (43)) is compared with the time delay feedback (14) of [19] in Fig. 14. As can be seen, both methods have equivalent damping performance in the first stage of the responses. However, analogously to the simulations in Fig. 11, the time-delay approach provides better damping in the second stage, approximately from $t > 5$[s]. As already discussed, it is caused by a constant amplitude Δl in (14). However as soon as the amplitude $\Delta\phi(t)$ gets below the process and measurement noise, this will lead to unpredictable jerky behaviour. Thus as soon as $\Delta\phi(t)$ gets below a predefined threshold, here we used $\Delta\phi_t = 0.1$[rad], the controller (14) must be switched off. This is not the case for the *control by force* feedback law which is entirely safe in this aspect.

The comparison of the proposed *control by force* feedback law (37), (43) with feedback law (19) of [24] is given in Fig. 15. One can observe that the control approaches provide

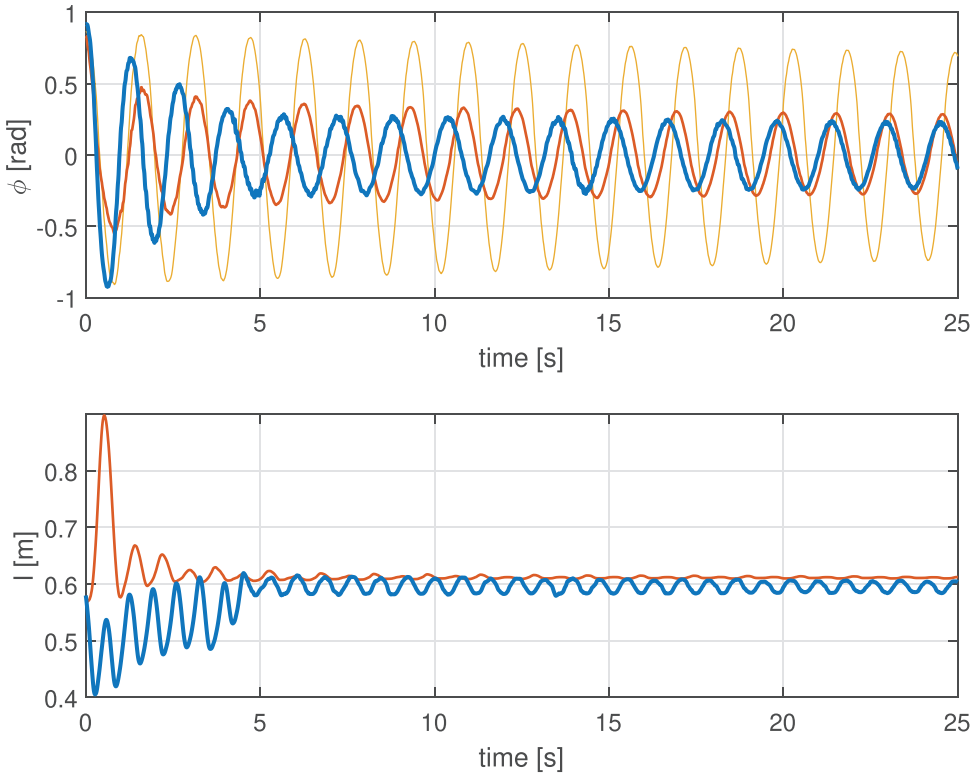

Fig. 15. Experiments: the time evolution of the pendulum angle and the pendulum length during the controlled swing. The blue line corresponds to newly designed force controller (37),(43), the red line to (19) of [24] and the yellow line to the uncontrolled swing. (For interpretation of the references to colour in this figure legend, the reader is referred to the web version of this article.)

almost equivalent damping of the pendulum. The main difference between the approaches can be observed in the evolution of the cable length. For the feedback (37), (43), the pendulum length oscillates around the nominal length and the amplitude of these oscillations decreases as the pendulum swing decreases. For the feedback (19) the length is significantly extended in the first phase. After the swing angle is reduced, it is shortened back to the initial length l_0 and continues to oscillate around this value. It should be noted that in a real-life crane set-up, this significant extension could be considered as a serious drawback. Mainly due to this aspect, and also due to straightforward implementation, the *control by force* feedback law designed using back-stepping should be preferred in practical applications. As a matter of fact, feedback law (37), (43) can be applied directly to a wide variety of crane set-ups as it contains only basic parameters such as the mass of the load and the required nominal length. On the contrary, feedback law (19) requires an additional PD block that needs to be tuned by a skilled control engineer at each occasion. It also applies in the comparison with the time delay feedback which cannot work within small angle variation.

6. Conclusions and outlook

This paper presented a progress towards model based feedback design for damping the swing of a pendulum by varying the suspension length. Future and ongoing research include, in particular, developing adaptive schemes accounting for cart and pivot friction which are currently estimated experimentally. To enhance the convergence speed, a hybrid control law may be considered, namely, switching to stronger gains when approaching the equilibrium. As an alternative, one can apply the backstepping technique twice to the smoothed feedback control law of Section 3.3. Last, but not least, an open theoretical question concerns how to take into account that the input force can only pull the cable, while the downward force is limited by the current value of the gravitational and centrifugal forces. In the laboratory experiments it was handled by adding saturation. Hence, the inclusion of saturation was successful in practice, yet a proper theoretical foundation is missing.

Declaration of Competing Interest

The authors declare that they have no known competing financial interests or personal relationships that could have appeared to influence the work reported in this paper.

CRediT authorship contribution statement

Milan Anderle: Investigation, Software, Visualization, Validation, Writing – review & editing. **Pieter Appeltans:** Investigation, Software, Visualization, Writing – review & editing. **Sergej Čelikovský:** Project administration, Funding acquisition, Investigation, Formal analysis, Writing – original draft. **Wim Michiels:** Formal analysis, Software, Investigation, Writing – original draft. **Tomáš Vyhlídal:** Funding acquisition, Supervision, Conceptualization, Methodology, Writing – original draft.

Acknowledgments

The presented research was supported by the Czech Science Foundation, project No. 21-03689S, through the collaboration projects VS.060.17N funded by the Research Foundation Flanders (FWO) and the Academy of Sciences of the Czech Republic and the collaborative project CELSA/20/013 funded by KU Leuven and the Czech Technical University in Prague in the framework of the CELSA alliance. The fifth author also acknowledges support from the ESIF, EU Operational Programme Research, Development and Education, and from the Center of Advanced Aerospace Technology (*CZ*.02.1.01/0.0/0.0/16_019/0000826), Faculty of Mechanical Engineering, Czech Technical University in Prague.

References

[1] E.M. Abdel-Rahman, A.H. Nayfeh, Z.N. Masoud, Dynamics and control of cranes: a review, Modal Anal. 9 (7) (2003) 863–908.

[2] W. Singhose, Command shaping for flexible systems: a review of the first 50 years, Int. J. Precis. Eng. Manuf. 10 (4) (2009) 153–168.

[3] T. Singh, T. Vyhlidal, Recent results in reference prefiltering forprecision motion control, Preprints of 21st IFAC World Congress, Berlin, Germany (2020) 12.

[4] D. Pilbauer, W. Michiels, T. Vyhlídal, Distributed delay input shaper design by optimizing smooth kernel functions, J. Frankl. Inst. 354 (13) (2017) 5463–5485.

[5] S. Nandi, T. Singh, Joint chance constrained input shaping, J. Frankl. Inst. 357 (14) (2020) 10027–10053.
[6] Z. Wu, X. Xia, Optimal motion planning for overhead cranes, IET Control Theory Appl. 8 (17) (2014) 1833–1842.
[7] Y. Fang, B. Ma, P. Wang, X. Zhang, A motion planning-based adaptive control method for an underactuated crane system, IEEE Trans. Control Syst. Technol. 20 (1) (2012) 241–248.
[8] K.L. Sorensen, W. Singhose, S. Dickerson, A controller enabling precise positioning and sway reduction in bridge and gantry cranes, Control Eng. Pract. 15 (7) (2007) 825–837.
[9] T. Vyhlidal, M. Hromcik, V. Kucera, M. Anderle, On feedback architectures with zero-vibration signal shapers, IEEE Trans Automat. Control 61 (8) (2016) 2049–2064.
[10] C.-Y. Chang, H.W. Lie, Real-time visual tracking and measurement to control fast dynamics of overhead cranes, IEEE Trans. Ind. Electron. 59 (3) (2012) 1640–1649.
[11] D. Chwa, Nonlinear tracking control of 3-d overhead cranes against the initial swing angle and the variation of payload weight, IEEE Trans. Control Syst. Technol. 17 (4) (2009) 876–883.
[12] H. Chen, Y. Fang, N. Sun, A swing constraint guaranteed MPC algorithm for underactuated overhead cranes, IEEE/ASME Trans. Mechatron. 21 (5) (2016) 2543–2555.
[13] L. Van den Broeck, M. Diehl, J. Swevers, A model predictive control approach for time optimal point-to-point motion control, Mechatronics 21 (7) (2011) 1203–1212.
[14] H. Ouyang, Z. Tian, L. Yu, G. Zhang, Motion planning approach for payload swing reduction in tower cranes with double-pendulum effect, J. Frankl. Inst. 357 (13) (2020) 8299–8320.
[15] D.S.D. Stilling, W. Szyszkowski, Controlling angular oscillations through mass reconfiguration: a variable length pendulum case, Int. J. Non Linear Mech. 37 (1) (2002) 89–99.
[16] W. Szyszkowski, D.S.D. Stilling, On damping properties of a frictionless physical pendulum with a moving mass, Int. J. Non Linear Mech. 40 (5) (2005) 669–681.
[17] S. Okanouchi, K. Yoshida, I. Matsumoto, H. Kawabe, Damping angular oscillations of a pendulum under state constraints, IFAC Proc. Volumes 41 (2) (2008) 7735–7742.
[18] A. Bellino, A. Fasana, E. Gandino, L. Garibaldi, S. Marchesiello, A time-varying inertia pendulum: analytical modelling and experimental identification, Mech. Syst. Signal Process. 47 (1) (2014) 120–138.
[19] T. Vyhlídal, M. Anderle, J. Bušek, S. Niculescu, Time-delay algorithms for damping oscillations of suspended payload by adjusting the cable length, IEEE/ASME Trans. Mechatron. 22 (5) (2017) 2319–2329.
[20] A. Rauh, R. Prabel, H. Aschemann, Oscillation attenuation for crane payloads by controlling the rope length using extended linearization techniques, in: Proceedings of the 22nd International Conference on Methods and Models in Automation and Robotics (MMAR), 2017, pp. 307–312.
[21] K. Yoshida, S. Okanouchi, H. Kawabe, Vibration suppression control for a variable length pendulum with a pivot movable in a restricted range, in: Proceedings of the 2006 SICE-ICASE International Joint Conference, 2006, pp. 4538–4544, doi:10.1109/SICE.2006.315085.
[22] K. Yoshida, H. Kawabe, K. Kawanishi, Stabilizing control for a single pendulum by moving the center of gravity. an investigation by numerical experiment, in: Proceedings of 35th IEEE Conference on Decision and Control, volume 1, 1996, pp. 1039–1040, doi:10.1109/CDC.1996.574631.
[23] K. Yoshida, I. Kawanishi, H. Kawabe, Stabilizing control for a single pendulum by moving the center of gravity: theory and experiment, in: Proceedings of the 1997 American Control Conference, volume 5, 1997, pp. 3405–3410, doi:10.1109/ACC.1997.612097.
[24] M. Anderle, W. Michiels, S. Čelikovský, T. Vyhlídal, Damping a Pendulum's swing by string length adjustment - design and comparison of various control methods, in: Proceedings of the 2019 American Control Conference (ACC), 2019, pp. 4399–4405.
[25] S. Čelikovský, M. Anderle, T. Vyhlídal, Underactuated pendulum damping by its length adjustment and passive output selection, in: Proceedings of the 2020 European Control Conference (ECC), 2020, pp. 100–105.
[26] C. Li, Z. Zhang, X. Liu, Z. Shen, An improved principle of rapid oscillation suppression of a pendulum by a controllable moving mass: theory and simulation, Shock Vib. 2019 (2019).
[27] C. Li, Z. Zhang, Z. Zhang, B. Wen, Experimental study of rapid oscillation suppression of a pendulum on the basis of intermittent mass motion, J. Vib. Control 26 (9–10) (2020) 840–850.
[28] M. Kuře, J. Bušek, T. Vyhlídal, S.-I. Niculescu, Algorithms for cable-suspended payload sway damping by vertical motion of the pivot base, Mech Syst Signal Process 149 (2021) 107131.
[29] C. Li, B. Zhu, Z. Zhang, W. Chu, Experimental study on rapid oscillation suppression of a pendulum using phase delay motion of pivot, Mech Syst Signal Process 158 (2021) 107757.
[30] Q. Wu, X. Wang, L. Hua, M. Xia, Modeling and nonlinear sliding mode controls of double pendulum cranes

considering distributed mass beams, varying roped length and external disturbances, Mech Syst Signal Process 158 (2021) 107756.
[31] M. Pinsky, A. Zevin, Oscillations of a pendulum with a periodically varying length and a model of swing, Int J Non Linear Mech 34 (1) (1999) 105–109.
[32] A. Zevin, L.A. Filonenko, Qualitative study of oscillations of a pendulum with periodically varying length and a mathematical model of swing, Prikl. Mat. Mekh. 71 (2007) 989–1003.
[33] A.O. Belyakov, A.P. Seyranian, A. Luongo, Dynamics of the pendulum with periodically varying length, Physica D 238 (16) (2009) 1589–1597.
[34] J. Zemánek, S. Čelikovský, Z. Hurák, Time-optimal control for bilinear nonnegative-in-control systems: application to magnetic manipulation, IFAC-PapersOnLine 50 (1) (2017) 16032–16039.
[35] J.J.B. Biemond, W.P.M.H. Heemels, R.G. Sanfelice, N. van de Wouw, Distance function design and Lyapunov techniques for the stability of hybrid trajectories, Automatica 73 (2016) 38–46.
[36] H. Lin, P.J. Antsaklis, Stability and stabilizability of switched linear systems: a survey of recent results, IEEE Trans. Automat. Control 54 (2) (2009) 308–322.
[37] H.K. Khalil, Nonlinear Systems; 3rd ed, Prentice-Hall, Upper Saddle River, NJ, 2002.
[38] S.S. Pavlichkov, S.N. Dashkovskiy, C.K. Pang, Uniform stabilization of nonlinear systems with arbitrary switchings and dynamic uncertainties, IEEE Trans. Automat. Control 62 (2017) 2207–2222.
[39] M. Krstić, I. Kanellakopoulos, P.V. Kokotovic, Adaptive nonlinear control without overparametrization, Syst. Control Lett. 19 (3) (1992) 177–185.
[40] D. Seto, A.M. Annaswamy, J. Baillieul, Adaptive control of nonlinear systems with a triangular structure, IEEE Trans. Automat. Control 39 (1994) 1411–1428.
[41] C. Rui, M. Reyhanoglu, I. Kolmanovsky, S. Cho, N.H. McClamroch, Nonsmooth stabilization of an underactuated unstable two degrees of freedom mechanical system, in: Proceedings of the 36th IEEE Conference on Decision and Control, volume 4, 1997, pp. 3998–4003.